Geomorphology xxx (2009) xxx–xxx

Contents lists available at ScienceDirect

Geomorphology

journal homepage: www.elsevier.com/locate/geomorph

DTM-based morphometry of the Palinuro seamount (Eastern Tyrrhenian Sea): Geomorphological and volcanological implications

Salvatore Passaro [a,*], Girolamo Milano [b], Claudio D'Isanto [a], Stefano Ruggieri [a], Renato Tonielli [a], Pier Paolo Bruno [b], Mario Sprovieri [a], Ennio Marsella [a]

[a] Istituto per l'Ambiente Marino Costiero (IAMC), Consiglio Nazionale delle Ricerche, Calata Porta di Massa, Porto di Napoli, 80133, Napoli, Italy
[b] Osservatorio Vesuviano, Istituto Nazionale di Geofisica e Vulcanologia, Naples, Italy

ARTICLE INFO

Article history:
Received 13 February 2009
Received in revised form 24 September 2009
Accepted 28 September 2009
Available online xxxx

Keywords:
Multibeam bathymetry
Marine volcanoes
Tyrrhenian Sea
Seamount
DTM

ABSTRACT

We present a high resolution DTM of the Palinuro Seamount (PS, Tyrrhenian Sea, Italy) resulting from the processing of multibeam swath bathymetry records acquired during the second leg of the "Aeolian 2007" cruise. PS consists of several superimposed volcanoes aligned along a N100°E strike and measures 55×25 km. The western and the central sectors result from the coalescence of collapse structures (calderas) with younger volcanic cones. The eastern sector reveals a more complex and articulated structure. In the central sector, a volcanic crater with a well-preserved rim not obliterated by erosional events suggests a volcanological rejuvenation of this sector. The presence of flat surfaces on the top of the seamount may be due to the formation of marine terraces during the last sea-level lowering. Lateral collapses on the northern and southern flanks of the seamount are probably related to slope instability, as suggested by the presence of steep slopes (25–40°). The main fault affecting PS strikes N65°E and shows a right lateral component of movement. E–W and N10°E striking faults are also present.

Assuming that the N100°E deep-seated fault, which is responsible for the emplacement of PS, moved with sinistral slips, we interpret the N65°E and the N10°E faults as right-lateral (second order) shear and left-lateral (third order) shear, respectively. Due to the particular location of the Palinuro Seamount, the data presented here allow us to better understand the volcanism and the geodynamic processes of the Tyrrhenian Sea.

1. Introduction

Although about 60% of the Earth's volcanoes is located in the marine environment, detailed morphological data are still poorly available, because of the intrinsic difficulties of marine remote sensing. Nonetheless, detailed side-scan sonar imaging and swath bathymetry are useful tools in the analysis of guyots (Smoot, 1995), shoaling volcanoes (McPhie, 1995) and seamounts (Smith et al., 1997), and allow us to understand constructional and erosional processes and active structural and volcanic processes (Moore and Mark, 1992; Rowland and Garbeil, 2000; Johnson et al., 2008). For example, the drainage pattern of volcanoes is often controlled by the presence of faults and dikes which, in turn, are responsible for and/or control collapse and spreading processes. In addition, reciprocal relations occur between the morphology of volcanic edifices, their substratum and the magmatic system (Thouret, 1999, and references therein).

In the last years, high resolution morphobathymetry (Mark et al., 1991; Gamberi et al., 1997; Marani et al., 2004; Gamberi et al., 2006) has been carried out in the Tyrrhenian Sea; the extensional back-arc basin located in the Central Mediterranean Sea. The recent multibeam bathymetric data acquired in the south-eastern Tyrrhenian Sea (Marani and Trua, 2002) has improved the knowledge on the Marsili Seamount, the largest ones in the Tyrrhenian Sea. This seamount, an almost linear edifice extending for about 55 km in the N15°E direction and characterized by a wide bathymetric range (3000–500 m), occupies the central sector of the Marsili ocean-like basin, the younger one of the Tyrrhenian Sea. The shape of this ocean-like basin is roughly circular and covers an area of ~8000 km^2 with a flat seafloor located at 3500 m bsl depth on average. The location of the Marsili Seamount, its relief and morphological characteristics have been explained in term of a super-inflated spreading ridge (Marani and Trua, 2002). A few kilometres northeastward from the Marsili Seamount is the Palinuro Seamount, which is also one of the largest in the Tyrrhenian Sea (Fig. 1). Despite its location, at the transition zone between the Aeolian volcanic arc (considered to be the arc system of the Ionian subduction in the Central Mediterranean Sea), the Marsili back-arc oceanic volcanism and the Southern Italy passive continental margin, and notwithstanding its length (about 50 km along the E–W direction), this seamount has not been subject to intensive geophysical exploration and is the least known volcanic complex of the southeastern Tyrrhenian Sea. Specifically, although recent high resolution morphobathymetric surveys were

* Corresponding author. Istituto per l'Ambiente Marino Costiero, Consiglio Nazionale delle Ricerche, Calata Porta di Massa, Porto di Napoli, 80133 Napoli Italy. Tel.: +39 81 5423831; fax: +39 81 5423888.
E-mail address: salvatore.passaro@iamc.cnr.it (S. Passaro).

0169-555X/$ – see front matter © 2009 Elsevier B.V. All rights reserved.
doi:10.1016/j.geomorph.2009.09.041

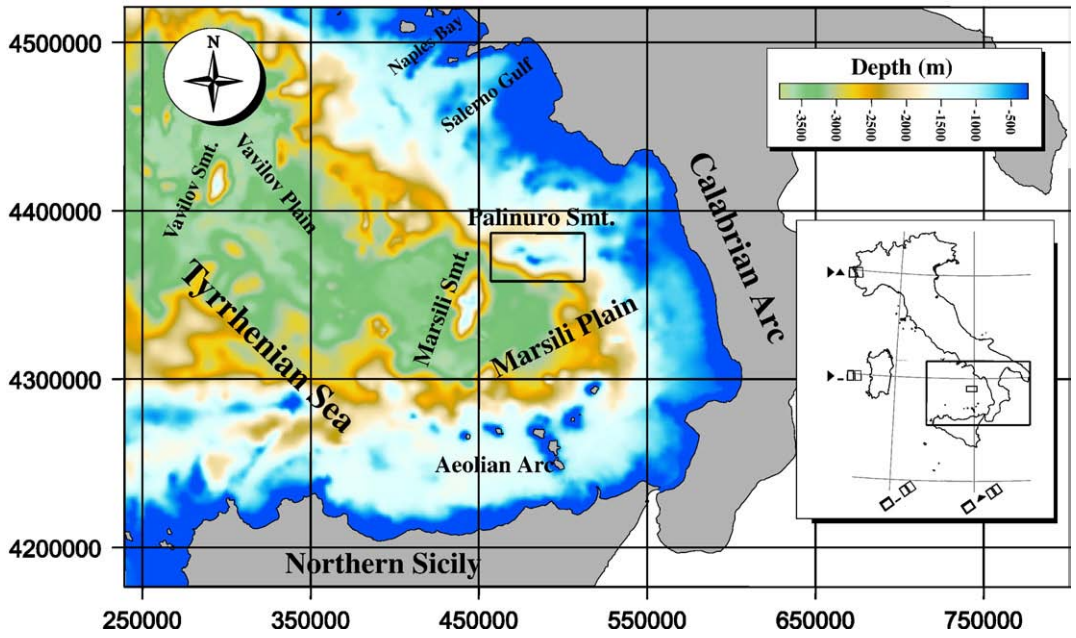

Fig. 1. Schematic map of the Tyrrhenian Sea and its main volcanic features. Scale colour indicates bathymetric depth. The Palinuro seamount is enclosed in a rectangle. (For interpretation of the references to colour in this figure legend, the reader is referred to the web version of this article.)

performed in the Eastern Tyrrhenian Margin (Gamberi et al., 1997; Marani et al., 2004; Gamberi et al., 2006), high resolution DTM and morphological analysis of the Palinuro Seamount have not been undertaken.

During the geophysical survey carried out by IAMC-CNR in the southeastern Tyrrhenian Sea on board of the R/V Urania on November 2007, whose aim was to identify potential active volcanic and/or hydrothermal vents, high resolution multibeam swath bathymetry was performed on the Palinuro Seamount. Here, we present a new, high resolution Digital Terrain Model (DTM) of the Palinuro Seamount built from the acquired data. On the basis of this dataset coupled with geomorphological and morphometric analyses of the volcano complex, we provide new insight on the role of the Palinuro Seamount in the context of the eastern Tyrrhenian Margin. In particular, we focus on: a) the relations between different volcanic landform and depth variations and b) the structural features. Due to its particular location at the transition zone between different crustal provinces bordered by major faults and deformation zones, we believe that the morphological analysis of the Palinuro Seamount may offer new significant elements for a better understanding of the regional volcanism and geodynamic processes in the southeastern Tyrrhenian Sea.

2. Geological setting of the Palinuro Seamount

The Palinuro Seamount (0.8–0.3 Ma; Beccaluva et al., 1982, 1985; Savelli, 2002; hereafter PS) is a volcanic complex located in the Tyrrhenian Sea (Fig. 1), a small extensional back-arc basin in the Central Mediterranean related to the subduction of the Ionian lithosphere below the Calabrian Arc in the context of the Africa–Eurasia convergence (Maliverno and Ryan, 1986). The opening of the Tyrrhenian Sea started about 11 My ago with an E–W-directed extension. This stage of evolution was characterized by widespread extension in the northern domain and rifting in the western part of the southern domain (Rosenbaum and Lister, 2004) and led to the formation of oceanic crust in the southern Tyrrhenian and the formation of the Vavilov (4.3 – 2.6 My; e.g. Kastens et al., 1990; Savelli, 2001) ocean-like basin. A subsequent change from E- to ESE-directed extension, coeval with frontal accretion in the Southern Appennines thrust belt, mainly affected the southeast Tyrrhenian Sea and led to the formation of the Marsili (1.8 – 0.2 My; e.g. Kastens et al., 1990; Savelli, 2001) ocean-like basin. This large-scale extension produced the onset of volcanism throughout the Tyrrhenian Sea and the surrounding coasts (Beccaluva et al., 1982, 1985; Turco and Zuppetta, 1998) and the formation of several seamounts. High values of heat flow (>150 mW m^{-2}; Della Vedova et al., 1984) and the thin crust (7 km on average) and lithosphere (30 km on average) (Suhadolc and Panza, 1989; Scarascia et al., 1994) testify to the young age of formation of oceanic crust in the Tyrrhenian Sea.

PS lies between the Marsili basin to the south, and the Southern Appenninic Chain to the east and it is bounded by a sedimentary basin to the north (Fig. 1). This zone represents the transition between the sedimentary shelf of the Salerno Gulf, which is the only sector characterized by the absence of volcanism, the Marsili ocean-like basin and the Aeolian Calcalkaline volcanism. The Southern Appenninic Chain represents a part of the arcuate orogenic belt including to the south the Calabrian Arc and the Sicily Maghrebides (Fig. 1) whose evolution is associated to the simultaneous subduction of a west-dipping lithospheric slab and the back-arc extension in the Tyrrhenian Sea (e.g. Malinverno and Ryan, 1986). The active volcanic Aeolian Archipelago, made up of seven major volcanic islands and several seamounts, form a ring-shaped structure that encircles the Marsili Basin from east to west. This last basin, according to De Astis et al. (2003), represents a post-collisional, rift-type volcanism emplaced in an older collision zone.

Although several geophysical studies have been performed in the Tyrrhenian Sea (Kastens, et al., 1988; Carminati et al., 1998; Gvirtzman and Nur, 1999; 2001; Argnani and Savelli, 2001; Faccenna et al., 2001; Savelli, 2001; Rosenbaum and Lister, 2004; Finetti, 2005; Goes et al., 2006; Montuori et al., 2007; Chiarabba et al., 2008), the PS has not yet been subjected to intensive geophysical exploration, thus representing the least known volcanic complex of the southeastern sector of the Tyrrhenian Sea. It is believed that PS is emplaced along a lithospheric fault that may represent the northward tear fault of the Calabrian Arc subduction (e.g. Guarnieri, 2006) but its role in the geodynamic context of the southeastern Tyrrhenian Sea is still debated. Due to the scarce geophysical information and the particular position occupied by PS in the Tyrrhenian Sea, some key issues are currently unresolved. Among the open questions, it is not clear if PS is: a) a part of the Aeolian Volcanic Arc (e.g. Finetti, 2005); b) independent from Aeolian Arc and controlled by pre-Pliocene tectonic structures (e.g. Guarnieri, 2006); and/or c) a flank volcano complex of the Marsili ocean-like basin (e.g. De Astis et al., 2003). In addition, the presence of swallow volcano-like seismicity

Please cite this article as: Passaro, S., et al., DTM-based morphometry of the Palinuro seamount (Eastern Tyrrhenian Sea): Geomorphological and volcanological implications, Geomorphology (2009), doi:10.1016/j.geomorph.2009.09.041

detected between PS and the Calabrian coast (Soloviev et al., 1990) suggests that PS, or its southeastern sector, could be active.

Previous studies on PS, focused mainly on volcanic products and were based on bottom sampling (Ciabatti, 1970; Del Monte, 1972; Fabbri et al., 1973; Marinelli, 1975; Di Girolamo, 1978; Kidd and Armansson, 1979; Dekov and Savelli, 2004 and references therein), mainly lavas and sediments associated with volcanism (i.e. crusts and iron- and manganese-bearing nodules). Magnetic profiles (Morelli, 1970) evidenced that the eastern sector of PS differs from the western one, the latter being characterized by widely ranging residual anomalies. Single beam data (Fabbri et al., 1973) and multibeam swath bathymetry (Mark et al., 1991; Marani et al., 2004) described the general physiographic characteristics of the volcanic complex, documenting a length of about 50 km along the W–E direction. A 3-D image of the seamount, obtained interpolating bathymetric data (Marani et al., 2004), shows two cones and an amphitheatre-like structure located to the west of them. According to Colantoni et al. (1981), PS was emplaced in a complex way and probably over a long period of time (0.5 Ma; Beccaluva et al., 1982, 1985; Savelli, 2002), along E–W striking and deep-seated fault system.

3. Data and methods

The geophysical survey for the present study was performed during the second leg of the "Aeolian_2007" cruise by the IAMC-CNR research institute (Naples, Italy) onboard the Urania oceanographic vessel in November, 2007. Multibeam data acquisition was carried out with the use of the Reson Seabat 8160 multibeam sonar system, which works well in the 50–3500 m depth range. The system, interfaced with a Differential Global Positioning System, is mounted on keel of the R/V Urania and is composed of a ping source of 50 kHz, 150° for the whole opening of the transmitted pulse and a 126 beams-receiver. The speed of sound in seawater was determined by a sound velocimeter profile. Sound velocity profiles were recorded and applied in real-time during the acquisition every 8 h.

Data have been processed according the following steps: (1) real-time acquisition control and partial beam filtering, applied to data directly on-board, on the basis of the experience of the operators (2) swath and spatial mode editing and de-spiking; and (3) DTM generation and rendering.

Systematic errors manifest as outliers in the bathymetric data, usually generated by acoustic and electronic factors (e.g. surface reflection, low signal-to-noise ratio due to bad weather conditions, etc; Mukhopadhyay et al., 2008). Errors affecting beam acquisitions (e.g. tilted swaths due to a wrong calibration, wrong positioning due to GPS "jumps", heave/pitch/roll/yaw-failed correction of the motion sensor, random false pikes in DTM due to poor acoustic beam detection or to the presence of obstacles along beam pattern, etc.) are reported in literature (Bourillet et al., 1996; de Alteriis et al., 2003).

The whole dataset has been processed with the use of the PDS2000 swath editor tool, in accordance with the IHO standard (IHO, 1998), and subsequently reorganized in an MXN matrix (Digital Terrain Model, DTM) of 25×25 m of grid cell size, where at each squared cell we associated the average value of beams that falls inside the cell itself. We completed the grid by simply associating a no-data value to empty cells. The total amount of area coverage consists of more than 1000 km^2 of multibeam sonar data. It is well known that, while vertical resolution depends only on the transducer frequency and water sound velocity, this is not the case of spatial (horizontal) resolution that is typically depth-dependent. Grid cell size of the DTM must be coherent with horizontal and vertical accuracy limits of soundings that are dependent on the intrinsic characteristics of the echosounder. Vertical accuracy is 2–8 cm for the Reson Seabat 8160 multibeam system used, and depends on the range utilized during the acquisition, while horizontal resolution is a function of depth and of the number of beams versus the swath opening, according to the equation:

$$Nf = D^{*}tg(SO / NB)$$

where: Nf = Nadir footprint, D = depth, SO = Swath Opening (in degrees), NB = Number of beams in the used array. Of course, nadir footprint is the smallest, and enlarges towards the external sectors of the swath.

The obtained DTM was used to produce standard computations, such as gradient, aspect, tangential curvature, profile curvature (Fig. 2A, B, C and D; Mitasova and Hofierka, 1993; Moore et al., 1993; Hodgson, 1998; Guth, 2003), openness (Fig. 2E; Yokoyama et al., 2002) and Standard Deviation maps (Fig. 2F).

4. Morphostructural features

The DTM of PS, with a depth range that covers the 3200–84 m below sea level (bsl) interval, is shown in Fig. 2, where a shaded relief image is reported. The DTM evidences a roughly elliptical shape extending about 55 km along N100°E and 25 km in the N–S direction. The morphology reveals a very articulated summit, characterized by different cone-like, flat and amphitheatre-like structures rather than a single volcanic edifice. Due to the structural complexity of the summit, we divide and separately describe three different DTM zones: a western zone (WZ), a central zone (CZ) and an Eastern zone (EZ) (Figs. 2 and 3). In the morphostructural sketch (Fig. 3) the most relevant volcanic elements are indicated with a capital letter.

Two structures are identified in WZ: A and B (Fig. 3). Feature A consists in a 4×4 km flat top surface, bounded to the west by a 50 m-high hill (Figs. 2, 4A). The feature A is limited by a 30° slope to the north, 25° to the south and 40° to the west (Fig. 4S), whereas a N60°E striking scarp is present on the southwestern flank (Fig. 4A). The top-depth is about 1600 m bsl. Feature B is characterized by a semi-elliptical shape, with a N115°E preferred orientation for the major axis. This feature extends 7.5×4.5 km at an average depth of 1200 m bsl, (Figs. 2, 3). This area is bounded by a crest, the depth of which ranges from 1200 (SSE) to 800 m (NW) bsl, and is abruptly interrupted in the NE part by a relief of about 500 m (Fig. 4B). The uppermost part of this relief is located at 500 m bsl. The slope angle of B is 15–20° in the northern and eastern scarps, 25° in the southern and 35° toward A (Fig. 4S).

The CZ feature is well developed. Two volcanic cones (C and D; Fig. 3), with flat circular tops of about 7–800 and 2500 m in diameter, respectively, are both characterized by a 30° slope-break value in all directions up to 1000 m (Fig. 4S). Structure C reaches 157 m bsl, whereas D represents the top of PS (84 m bsl). C and D top surfaces dip gently toward WNW. The presence of these two cones was previously reported by Fabbri et al. (1973) and Marani et al. (2004) (we propose the name "Piotr's cones" for these two edifices in honour of the researcher Piotr Mikejcik of the IAMC-CNR of Mazara del Vallo, who lost his life in the Sicily seas during the sinking of the Thetis oceanographic vessel, on the 3rd of August 2007). Three other cone-like reliefs can be recognized in CZ: E, F and G. E, characterized by a roughly crater-like top which extends for about 2.1 km^2 and shows flanks strongly marked by the presence of morphostructures with a N10°E and N115°E preferred orientations, whereas the western margin seems bounded by a N–S trending structure (Figs. 2, 3). In its central part, this edifice shows a crater with a bottom 75 m deeper than the top border, the latter being located at 570 m bsl (Figs. 2 and 4E). Relief F shows an elliptical shape with a N110°E elongated major axis (Figs. 2 and 3) characterized by a multifaceted top surface. The latter is located at 600 m bsl and seems strongly tilted toward N297°E, with a N30°E structural fabric (Fig. 4F, S). G shows a semi-circular shape with a very flat top at 1120 m bsl (Fig. 4G).

The main feature of the EZ is the presence of a relative high (H) placed at 950 m bsl, showing an elliptical shape elongated N110°E, with major and minor axes of 6000 and 4500 m, respectively (Fig. 3). The well defined top, H, is marked by a N–S/N10°E distinct ridges (Figs. 2, 3, 4H) whereas southeastward it progrades to a sector of the slope where a border of detachment is discernible (Fig. 3).

Please cite this article as: Passaro, S., et al., DTM-based morphometry of the Palinuro seamount (Eastern Tyrrhenian Sea): Geomorphological and volcanological implications, Geomorphology (2009), doi:10.1016/j.geomorph.2009.09.041

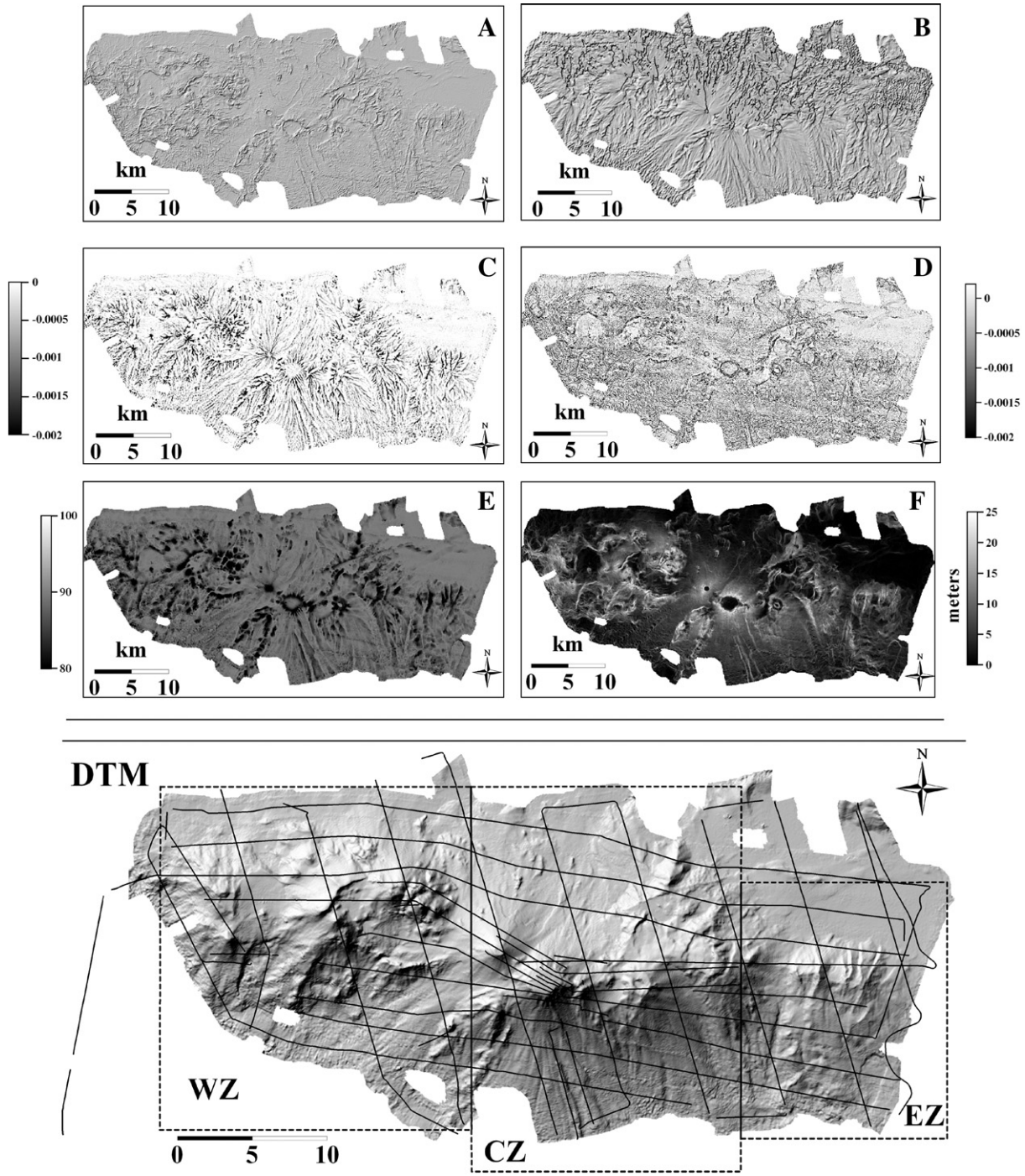

Fig. 2. DTM of the Palinuro seamount, obtained from processing of Multibeam swath bathymetry acquired during the second leg of the Aeolian_2007 cruise (2007, November), and navigation patterns. Grid cell size is 25 m. Geo-referencing system: Datum WGS84, projection UTM (zone 33). Morphometric computations carried out on DTM are also shown: gradient (A), aspect (B), tangential curvature (C), profile curvature (D), openness (E) and Standard Deviation (F) maps.

5. Morphological features and interpretation

The processed bathymetric data reveal previously unreported topographic features of PS both below 1000 m bsl and for the summit. The summit is very articulated and characterized by the presence of distinct volcanic structures. Unlike other seamounts that show almost continuous summit regions along their main axis (e.g. Marsili; Marani and Trua, 2002). The most important topographic features are found in WZ. The general shape of A and B, marked by a flat-topped surface and steep slopes of the sidewalls, suggest that these structures are calderas (Figs. 2, 4A, B). The very flat top morphology of A suggests that this caldera is filled by fine sediments. The B topographic features indicate that this could be a caldera affected by a lateral collapse due to the presence of a residual rim particularly evident towards the NW and from S to SE with respect the centre of B (Fig. 4B). The compound NE rim of B has been structurally modelled by erosion and by roughly N60°E faults. The southwestern scarp of B shows a composite morphology interpreted as ridges formed by erosion (Figs. 2, 4B).

The major topographic features in CZ are the presence of the two Piotr's cones and volcanic edifice E. The flat-topped surfaces of the minor (C) and the major (D) Piotr's cones (Figs. 2, 4S) can be explained as the result of the exposure to erosion during the last eustatic low-stand

Please cite this article as: Passaro, S., et al., DTM-based morphometry of the Palinuro seamount (Eastern Tyrrhenian Sea): Geomorphological and volcanological implications, Geomorphology (2009), doi:10.1016/j.geomorph.2009.09.041

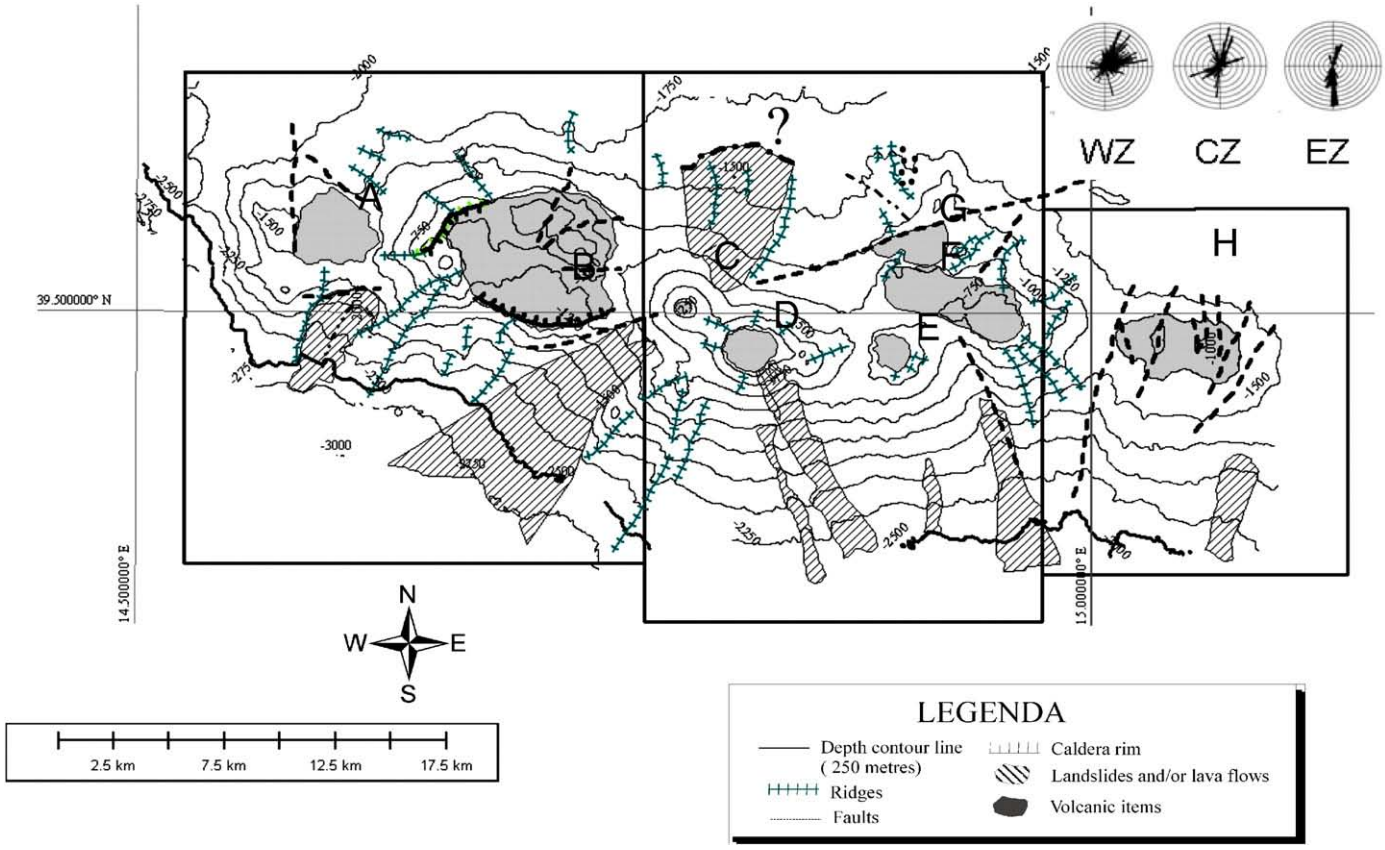

Fig. 3. Morphostructural sketch of the Palinuro seamount, interpreted on the basis of DTM. WZ, CZ and EZ divided the structure into three sectors, capital letters refer to the major volcanic features identified (see text for details). Rose diagrams on the upper-right corner of the picture represent aspect by slope computations of WZ, CZ and EZ.

(120 m at 19 ka, Lambeck et al., 2004). This assumption is corroborated by Ciabatti (1970) and Fabbri et al. (1973), who suggested the presence of marine terraces over the top of Piotr's cones due to erosional processes. The southwestern margin of Piotr's cones replicates the SW margin of the WZ, with the presence of ridges. The E cone is the only edifice that clearly shows a pronounced crater (Figs. 2, 4E), suggesting a relatively young formation for E. The general observations on E and Piotr's cones suggest that CZ is volcanologically younger than WZ.

Apart from its size, the general shape of G (characterized by a very flat-topped surface suggesting the presence of fine grained sediment infilling), is quite similar to A, the latter being located in the WZ (Fig. 4A, G, and S). Another common element is small hills, similar to small cones 50–75 m high, that are detected on both the A and G features.

These observations on both G and A resemble the morphological features of mud volcanoes (Gardner, 2001). It is well known from literature (e.g., Charlou et al., 2003) that mud volcanoes are volcano-sedimentary features, mainly (but not only) concentrated in compressional tectonic settings, characterized by the emission of fluid-rich fine grained sediments often associated with mud breccia. Altough mud breccia recognition is a critical issue for their identification, marine mud volcanoes can be initially detected with multibeam or side-scan data soundings on the basis of records with high values of backscattering (e.g. Huguen et al., 2005; Zitter et al., 2005). Therefore, our hypothesis that A and G are mud volcanoes must be validated by other geophysical investigations, in particular from bottom samplings, side-scan sonar and reflection seismic data that we plan to acquire in a future survey. Alternatively, since mud volcanoes are uncommon in volcanic settings, A and G could be hydrothermally altered deposits (e.g. hot springs, mud pots, fumaroles) or pillow lavas rather than true mud volcanoes.

Both the northern and southern margins of the CZ would seem to have been subject to episodes of gravitational events, e.g. lateral collapses. The morphology clearly shows signs of at least two major structural discontinuities, striking roughly N–S and N65°E (Figs. 2, 3), that could have guided sliding processes on the CZ flanks (Fig. 3). The above general features suggest that the cones inside the CZ are placed over a semi-elliptical continuous margin (Fig. 2), in agreement with a previous interpretation of this zone for which a horse-shape caldera (Bonatti et al., 1997) has been inferred.

6. Morphometry and volcano-tectonic features

Unlike the Aeolian seamounts, PS has a very asymmetrical and elongated shape. In order to define properly its regional trends, we built a stack of profiles perpendicular (Fig. 5A) and parallel (Fig. 5B) to the main N100°E elongation of PS. The plot of results shows different erosional base level values both for E and W (1592 and 2750 m bsl, respectively) and for N and S (1872 and 2530 m bsl). This evidence can be easily interpreted taking into account that the wider PS structure is emplaced at the transition between the Marsili Plain (W, SW and S margins) and the continental escarpment (E margin). Northward, the presence of other structures may have contributed to the formation of a sedimentary basin, creating a sort of physiographic sedimentary trap bounded southward by PS, as confirmed by ETOPO1 (Amante and Eakins, 2008) low resolution bathymetric data (Fig. 6).

Real average values of erosional base levels and general trends established through the stack of profiles are quantifiable through elevation histograms, which consist in a simple plot of elevation versus percentage of the area, where the maxima are related to flat surfaces of the DTM. In our case, such surfaces mainly indicate erosional base levels for deeper depth values, and erosional terraces for the shallowest. We have completed histogram elevation plots for each zone separately and for the whole PS (Fig. 7). EZ (Fig. 7a) and the whole PS (Pal in Fig. 7) show a clearly visible peak in correspondence at 1582 m bsl depth, which

Please cite this article as: Passaro, S., et al., DTM-based morphometry of the Palinuro seamount (Eastern Tyrrhenian Sea): Geomorphological and volcanological implications, Geomorphology (2009), doi:10.1016/j.geomorph.2009.09.041

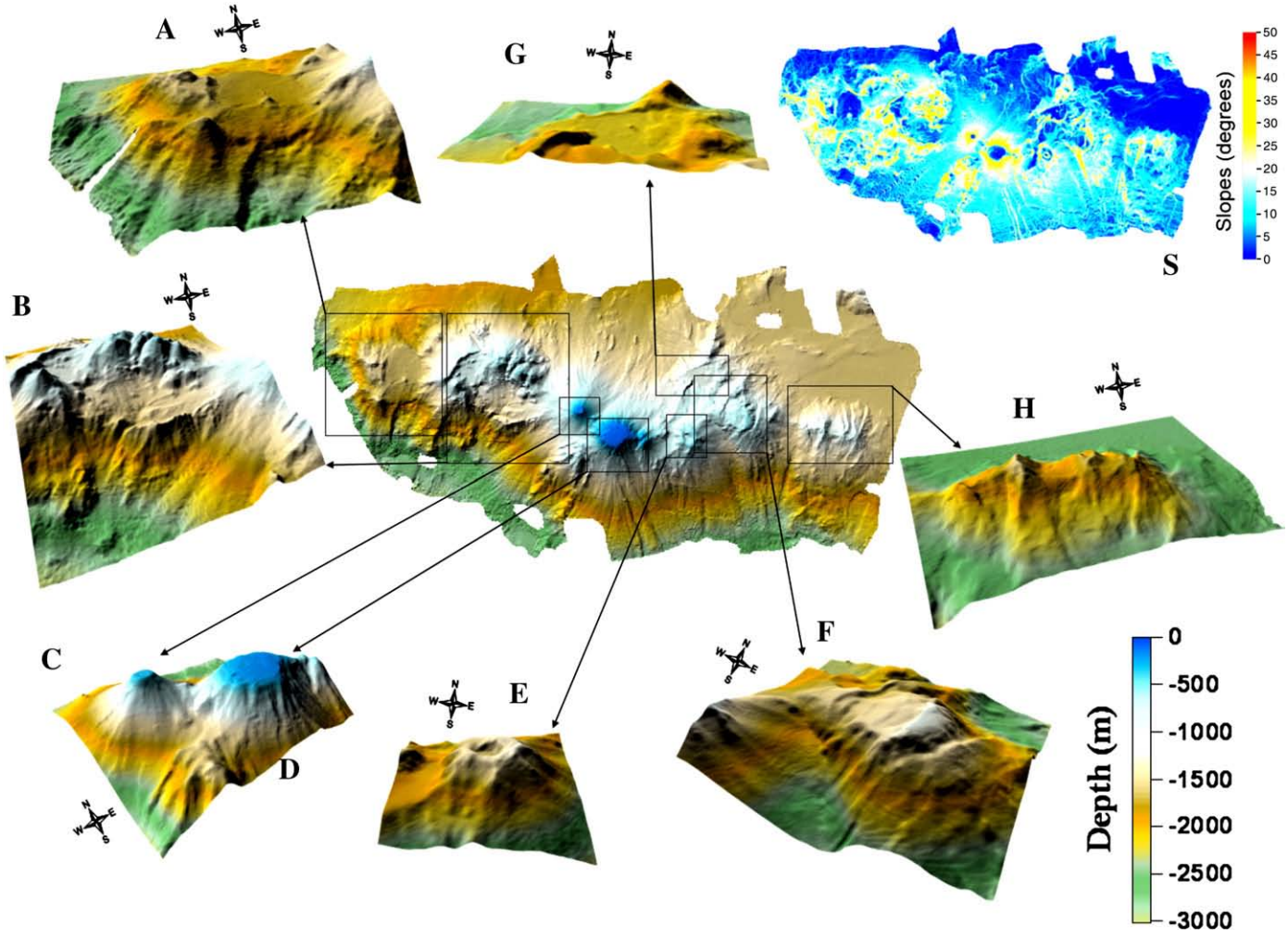

Fig. 4. Three-dimensional representation of the Palinuro seamount main features, corresponding to the capital letters of Fig. 3. Vertical exaggeration is 2× with respect to the horizontal component for all of the represented subsets. S, in the right-top corner, represents the slope map, reported in true degrees.

represents the northern erosional base level for the Palinuro Seamount (Figs. 3, 4S and 5). WZ (Fig. 7c) is characterized by the presence of other maxima of depths of 1870, 2195 and 2807 m bsl. The deepest of these values is related to the WZ southern erosional base level (not covered by data in CZ and EZ), while the others indicate the presence of flat morphologies that are not evident from inspection of shaded relief images, lying eastward (2195 m bsl) and northward (1870 m bsl) with respect to A. The observed differences between elevation histograms of the different sectors confirm the hypothesis suggested from the magnetic data (Morelli, 1970) of a substantial difference existing

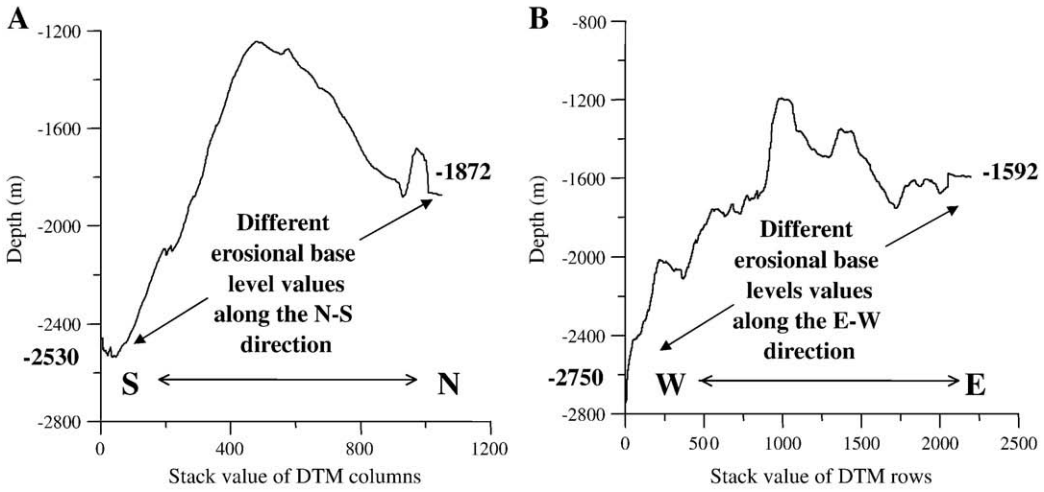

Fig. 5. Stack of profiles along E–W and N–S direction, showing respectively the large-scale distribution of the Palinuro seamount perpendicularly (A) and parallel (B) to the main E–W oriented volcanic ridge. Abscissas are progressive cell numbers, ordinates are depth in metres.

Please cite this article as: Passaro, S., et al., DTM-based morphometry of the Palinuro seamount (Eastern Tyrrhenian Sea): Geomorphological and volcanological implications, Geomorphology (2009), doi:10.1016/j.geomorph.2009.09.041

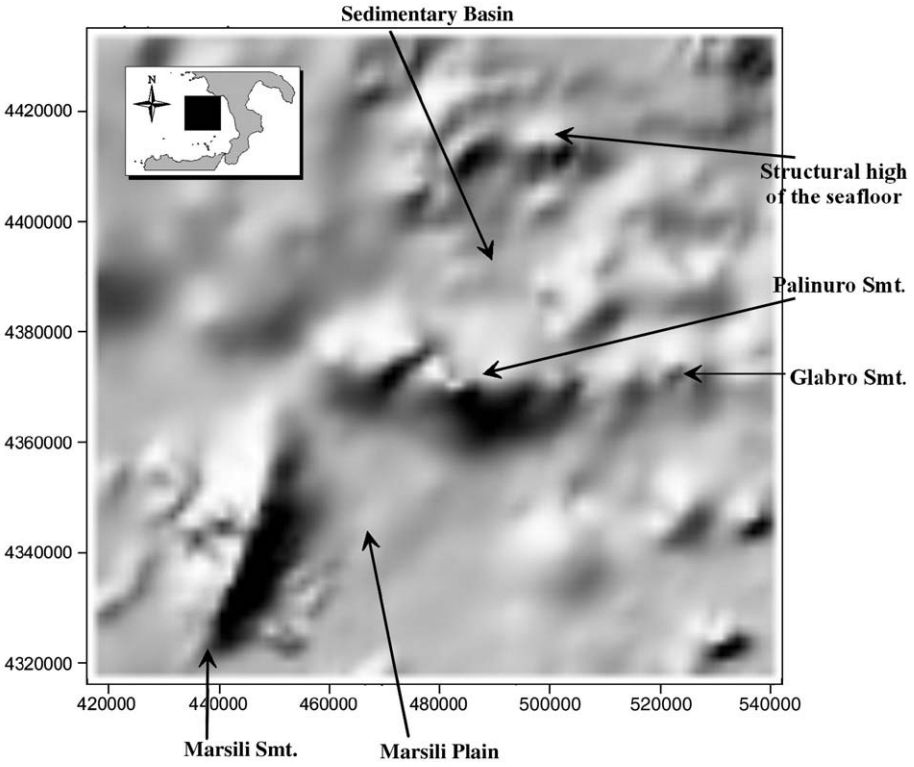

Fig. 6. Low resolution predicted satellite bathymetry map (Amante and Eakins, 2008) of the Palinuro seamount and of the surrounding area. The Palinuro structure is emplaced both on the boundary of the Marsili Plain (W, SW and S margins) and on the continental escarpment (E margin).

between EZ, mainly consisting in a single volcano, and CZ, consisting of a volcanic complex (see Figs. 3, and 4).

In order to appreciate the role of distinct depth values, we estimated the elevation versus average slope of PS, where slopes are located as a function of depth at which they occur. The resulting plot (Fig. 8A) recognizes 4 maxima or minima. Minima values evidence the erosional base levels (Fig. 8A: Point 3 = northern erosional base level, 1582 m bsl; Point 4 = southwestern erosional base level, 2807 m bsl)

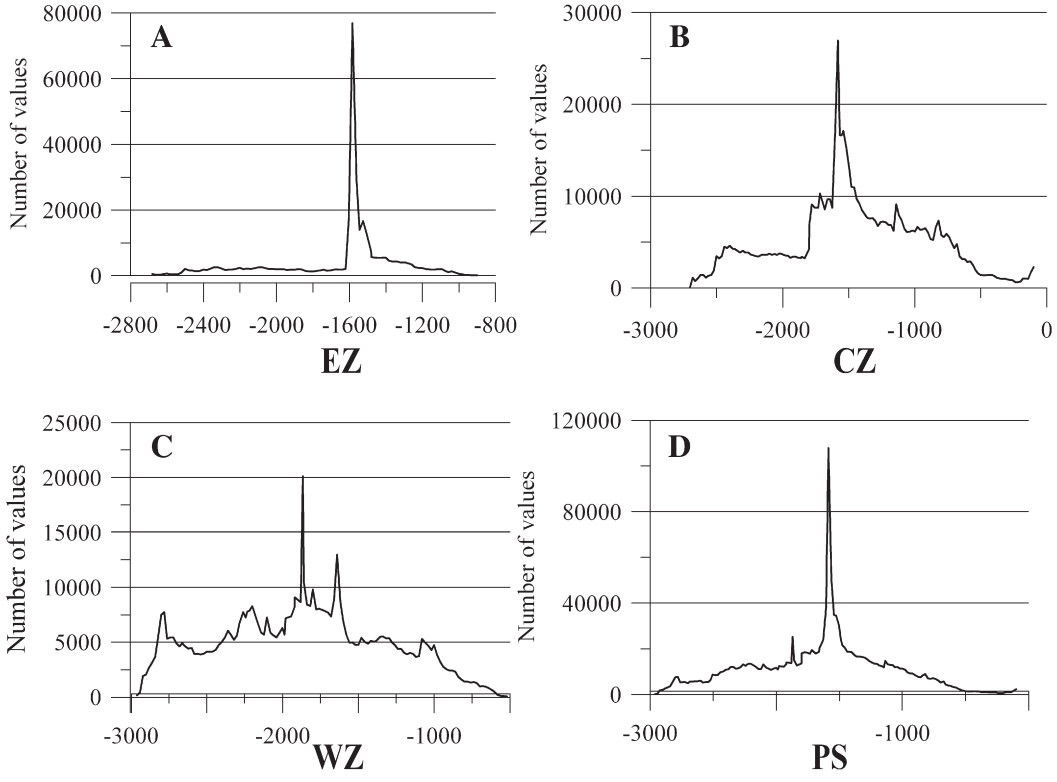

Fig. 7. Elevation histograms of EZ, CZ, WZ and of the whole PS.

Please cite this article as: Passaro, S., et al., DTM-based morphometry of the Palinuro seamount (Eastern Tyrrhenian Sea): Geomorphological and volcanological implications, Geomorphology (2009), doi:10.1016/j.geomorph.2009.09.041

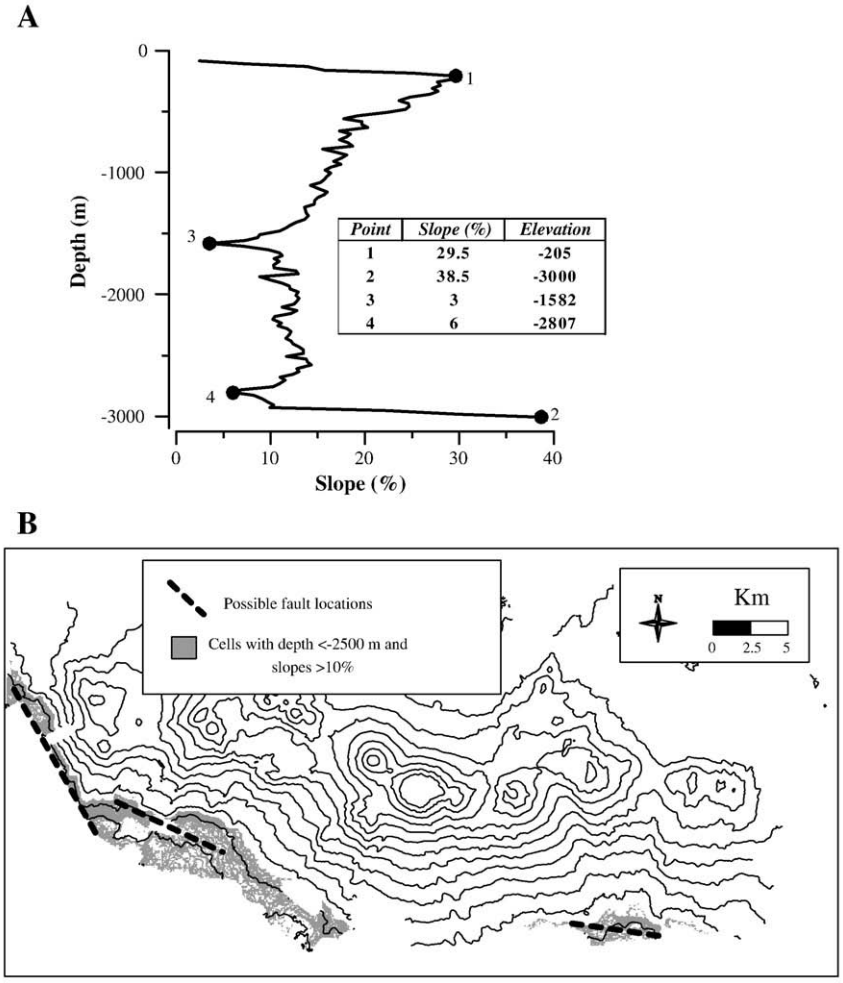

Fig. 8. A): Elevation versus slope plot. B): possible locations of faults inferred by the locations of steepest (>10°) and deepest (>2500 m bsl) values of DTM.

already identified from previous analysis (Fig. 7a, c). Maxima are located at 205 m (30%; point 1 in Fig. 8A) and at 3000 m bsl (40%; point 2 in the same figure). Point 1 is related to the abrupt slope-break of Piotr's cones top terraces, these being the shallowest features of PS (Fig. 4C, and D). As regard to the deepest high slope value (Fig. 8A, point 2), this is related to a southern scarp, i.e. the northern boundary of the Marsili Plain. In this picture, the presence of this steep scarp suggests the occurrence of a fault. The fault scarp may be inferred by plotting steep (>10%) and deep (<2500 m bsl) values in the DTM (Fig. 8B).

7. Discussion

According to McPhie (1995) and Head and Wilson (2003), marine volcano products, variations in the eruption and fragmentation processes are influenced by water depth. The comparison between DTM, stack of profiles and a profile extracted over the ridge of DTM may clarify some aspects of the evolution of PS (Fig. 9). Differently from other sectors, WZ is characterized by concave profiles and strongly dissected morphologies bounded by ridges (caldera and craters) and volcano-tectonic depressions (Fig. 4B). This peculiar characteristic allows us to infer that WZ probably represents the older part of the seamount, where both vertical (caldera) and lateral features (landslides) are clearly visible in the morphologies.

The CZ has well-delineated cones and edifices. C, D, E, G and the deepest portion of F display an amphitheatre-like structure (Fig. 3). The WZ and G are downward shifted with respect to CZ (Figs. 7a, b, and 10B). F shows a conical-shape (see Figs. 3 and 4F) and is dissected by N–S structures on its top. Southern and northern CZ escarpments are strongly incised by channels and valleys (Figs. 2 and 3). In the southern escarpment of CZ, in particular, these features are remarkably extended (15 km). Incision of these channels could have been enhanced by gravitative phenomena, such as slides. The flat-topped surfaces of the minor (C) and the major (D) Piotr's cones (Figs. 2 and 4S) can be explained as the result of the exposure to erosion during the last eustatic low-stand (120 m below the actual sea level; Lambeck et al., 2004). An apparent continuity between C and D (Piotr's cones) seems evident from elevation profiles (Fig. 10A). Such elevation continuity between relief is a typical effect related to the development of sea-level high-stand terraces, which occur when surfaces are related to the same episode of sea level.

It is well known that rock alteration and high fluid pressure characterize hydrothermal activity (that have been monitored on the top of the PS; see Dekov and Savelli, 2004 and references therein). This activity can weaken a volcanic edifice, contributing strongly to an increase in slope instability (Cecchi et al., 2005). These elements may suggest that some of the CZ valleys could have been produced by lateral spreading phenomena (gravitational valleys; Carracedo, 1996; Thouret, 1999), although hummocky facies are present but not noticeable on the southern side of CZ (Fig. 10E). The absence of such facies are probably due to the distinctive characteristics of the materials involved in lateral collapses (e.g. mud flows generate mounded rather than hummocky facies in the zone of accumulation) or to the lack of a proper cover of the southern erosional base level. As regards the existing reciprocal relations between drainage patterns of WZ, CZ and EZ and (hypothized) associated controlling

Please cite this article as: Passaro, S., et al., DTM-based morphometry of the Palinuro seamount (Eastern Tyrrhenian Sea): Geomorphological and volcanological implications, Geomorphology (2009), doi:10.1016/j.geomorph.2009.09.041

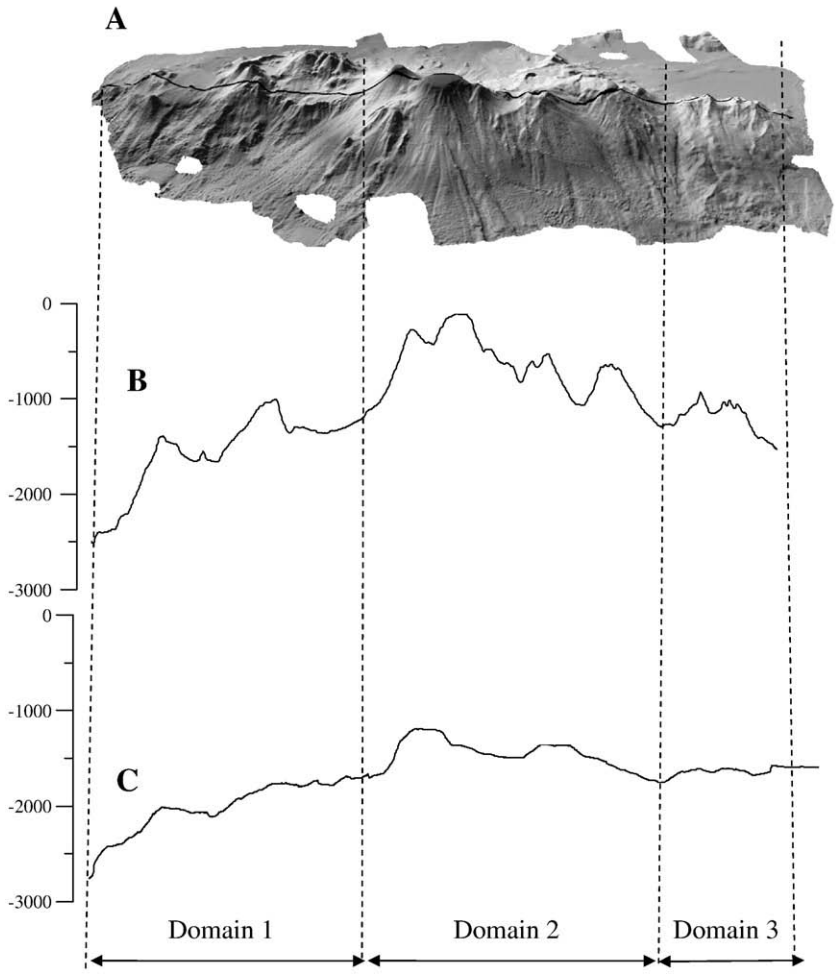

Fig. 9. Different volcano tectonic styles along the EW direction, enhanced through DTM (A), ridge elevation profile (B) and the stack of elevation profiles along columns (C). Domain 1 (WZ) is characterized by deep and ancient volcanism, Domain 2 (CZ) by most recent volcanic shapes. Domain 3 (EZ) seems strictly constrained by fractures.

structures, we have reported (Fig. 3) a rose diagram distribution of drainage aspects. In order to expand these considerations, we evaluated the drainage aspects with respect to slope, assuming that low angles are representative of the general regional trends of the structures, while high angles represent the main ridges and channels, which are probably related to active structures. A lack of symmetry is enhanced (Fig. 11), due to different erosional and volcanic styles. In detail, low slope values (0–10%) are mainly southward oriented in EZ (Fig. 11, EZ) and eastward in WZ (Fig. 11, WZ), while higher slope values (>30%) are mainly southeastward oriented in WZ and EZ, and southward in CZ (Fig. 11, CZ).

On the basis of the above results, we stress that the overall morphology of PS clearly shows evidence of structural fabric oriented in different directions. Segments of roughly N–S structures are identifiable on the top of H within EZ (Figs. 2, 4H). The general morphological feature of EZ suggests that this sector could be an element of transition toward the Glabro seamount, lying eastward (Fig. 1) and close to the mainland. N–S oriented structures are found also in CZ whereas roughly ENE–WSW oriented structures are found in WZ and CZ (Figs. 2, 3). The most important fault strikes N65°E and cuts CZ and the borders B towards the SW and G towards the NE (Fig. 3). This structure physiographically separates two sectors of PS that differ morphologically. In other words, this fault could be regarded as the dividing line between the most ancient (NW) and the younger (SE) sectors. Ocean-bottom seismographs operating in the Southeastern Tyrrhenian Sea in 1987 recorded several shallow volcano-type microearthquakes ($M_l < 3$) located between the SE scarp of PS and the Calabrian coast (Soloviev et al., 1990). The presence of this seismic activity, not detected on the near mainland of the Calabria Arc, suggests that EZ of PS could be active.

Although it was proposed that E–W trending deep-seated faults have controlled the general PS emplacement (Colantoni et al., 1981), the N65°E fault may have controlled the arrangement of the younger part. DTM-based evidence suggests a right lateral component of movement for such N65°E fault, since it displaces two segments of a unique ridge-like shape (Fig. 12).

The N65°E and the N100°E faults detected on the DTM of PS, could be related to the kinematic of the E–W deep-seated structure that have controlled the emplacement and the evolution of the whole Seamount. Considering that PS align along a N100°E and assuming that the E–W deep-seated structure moved as a sinistral strike–slip system (e.g. Savelli, 2001; Mantovani et al. 2008), according to the model proposed by Flodin and Aydin (2004), structure evolution of the PS could be interpreted as a conjugate fracture system with different generation of fractures. In this fault-network evolution model, based on a sequential opening-mode fracturing, each generation appears to have formed in response to deformation of earlier generation fractures. Higher-order fault generations are generally younger and show about five to ten times less slip than the generation preceding it. Therefore, the E–W deep-seated structure could be interpreted as the main fracture (the oldest) of the network, the N65°E fault can be interpreted as a second generation of faults, characterized by a right-lateral component of movement. The

Please cite this article as: Passaro, S., et al., DTM-based morphometry of the Palinuro seamount (Eastern Tyrrhenian Sea): Geomorphological and volcanological implications, Geomorphology (2009), doi:10.1016/j.geomorph.2009.09.041

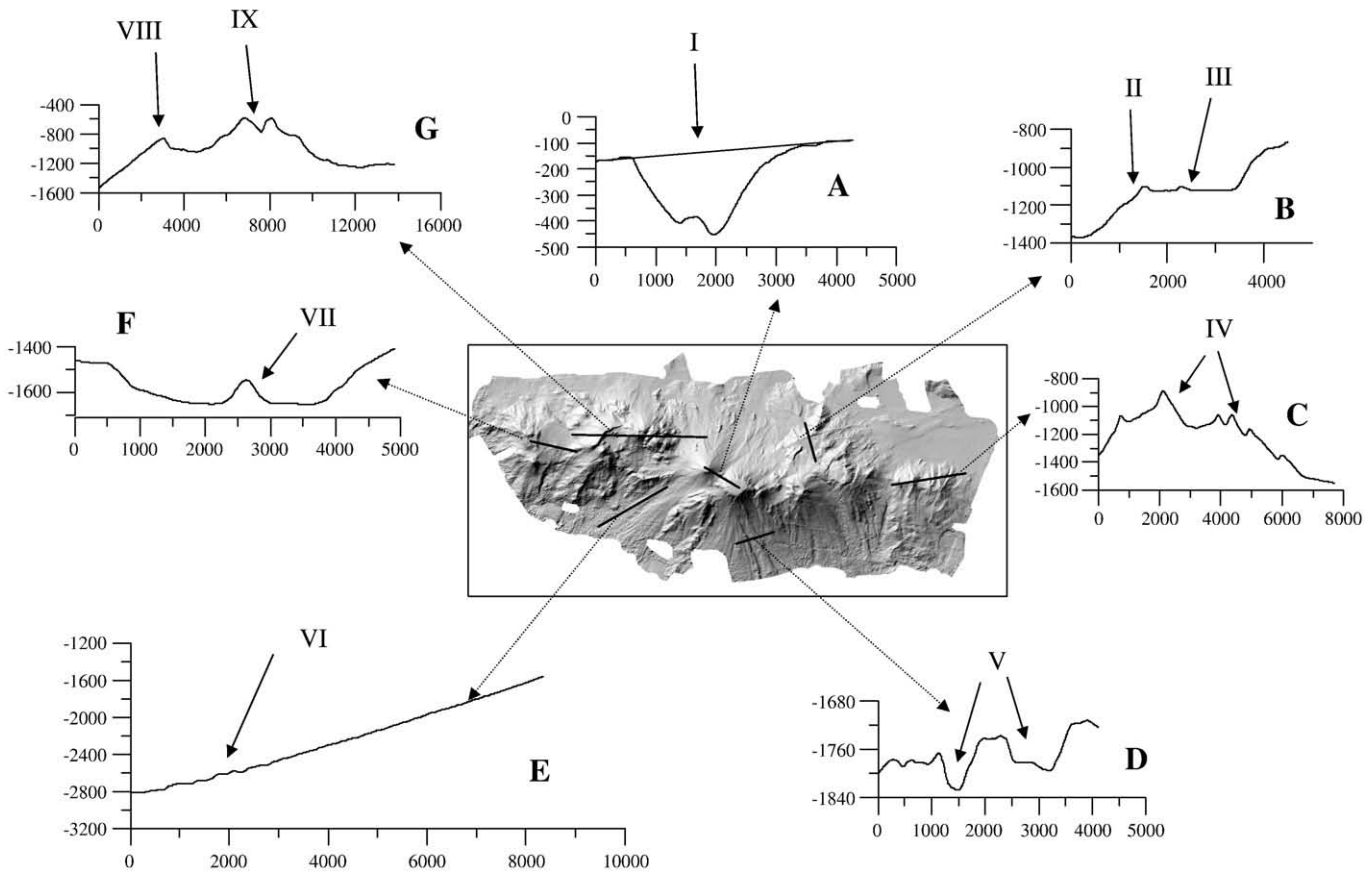

Fig. 10. Depth profiles extracted by DTM. I) Line of sight connecting C and D (Piotr's cones). Slope = 1.1°; II) N65°E fault and III) G flat surface; IV) Evidence of structures identifiable on the top of H (EZ); V) Channels excavated by lava flows/marine landslides; VI) Zone of accumulation of marine landslides on the valley which separates WZ and CZ; VII) Internal relief (roughly 70 m) inside A; VIII) Relic of caldera rim and IX) Relief (rejuvenation) bordering the B feature. Abscissas are true horizontal distances (in m), ordinates are depth (in m).

N–S fault system (e.g., EZ) could be either related to: 1) the accommodation space of the E–W first generation left-lateral deep structure, and then interpreted as a second generation of faults; or 2) as left-lateral faults related to right-lateral movement of the N65°E second generation, thus representing a third generation of faults. Since spacing and length of structures in this model depend on structural hierarchy, and the N–S

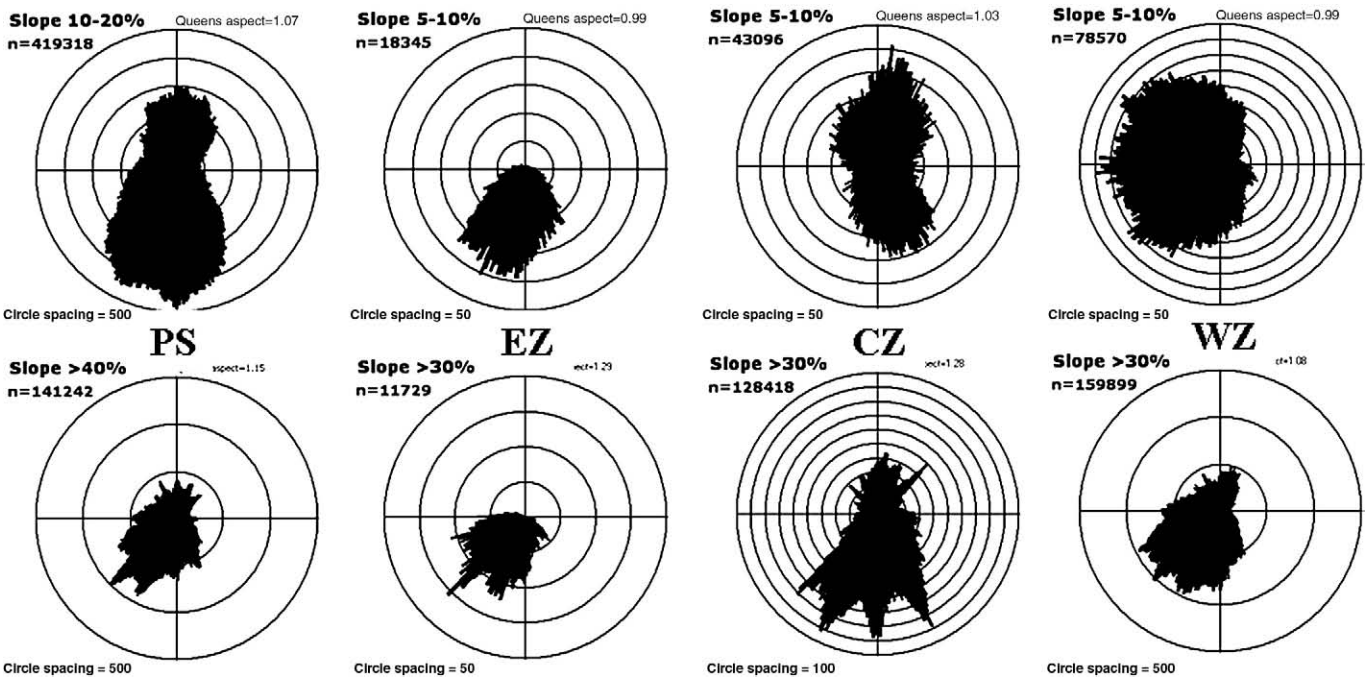

Fig. 11. Aspect distribution by slope for the PS and for EZ, CZ and WZ, showing low angle (above) and high angle (below) aspect distribution.

Please cite this article as: Passaro, S., et al., DTM-based morphometry of the Palinuro seamount (Eastern Tyrrhenian Sea): Geomorphological and volcanological implications, Geomorphology (2009), doi:10.1016/j.geomorph.2009.09.041

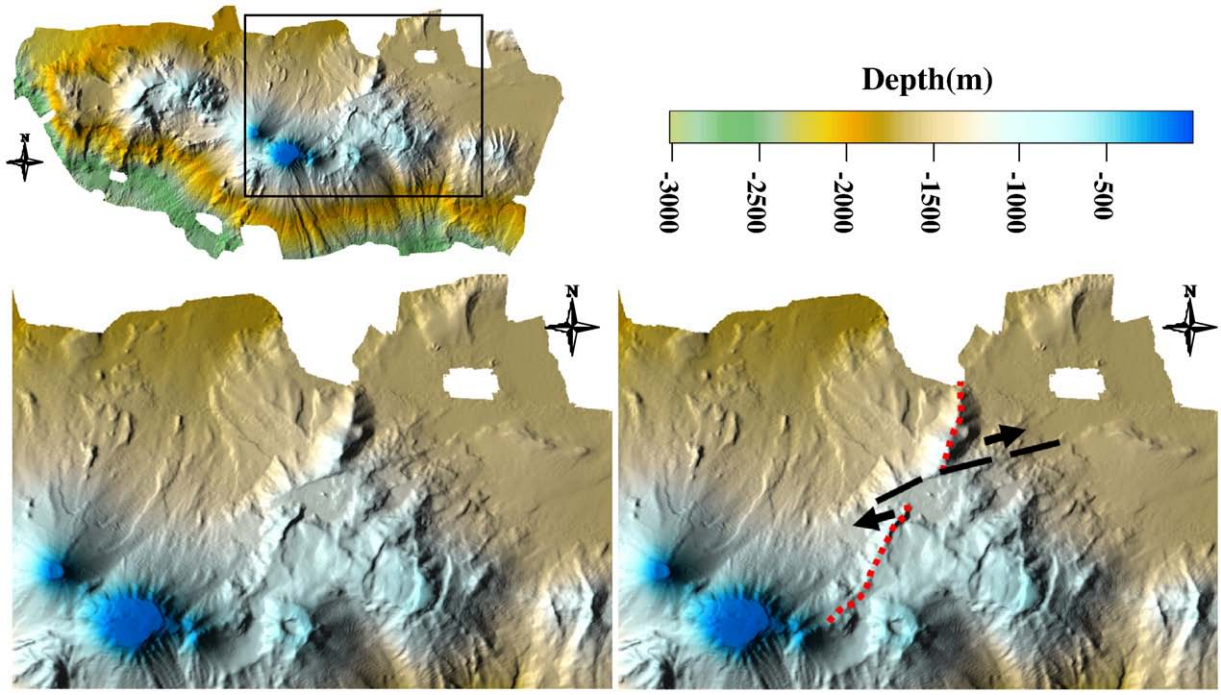

Fig. 12. Effect of the right-lateral component of movement of the N65°E fault of the PS.

structures tend to have smaller spacing and length attributes (e.g. WZ, Fig. 3), we favour the second hypothesis.

8. Concluding remarks

More than 1000 km^2 of new multibeam sonar data have been processed and interpreted. Data interpretation has been coupled with morphometric analysis of a DTM. The main results of the work can be summarized as follows:

- PS is characterized by a roughly elliptical shape extending for about 55 km along E–W and 25 km in N–S directions. Its summit is very articulated and consists of a group of overlapped and/or coalescent volcanic edifices, that we have interpreted as a sequence of volcanic cones inside collapsed calderas. Relic ridge-like shapes (maybe related to calderic collapses) are identifiable both in the central and in the western sectors of PS. Relic calderic rims are identifiable in the central sector of the seamount.
- The most important previously unknown volcanic structures are found in the western sector, characterized by the presence of two calderas, one of which is perhaps attributable to hydrothermally altered deposits (e.g. hot springs, mud pots, fumaroles) or pillow lavas. This sector appears to be the oldest one.
- The central sector is characterized by distinct volcanic structures. Although their existence has been known from previous geophysical investigations, a previously unreported element is that one of these clearly shows a volcanic crater with a pronounced rim not obliterated by erosional events, suggesting this sector is the younger one of the whole PS.
- The eastern zone seems to be completely different from the other zones, being structurally controlled and representing a potential element of transition toward the mainland.
- Different erosional base levels are found both in the N–S and E–W directions. Different volcanic styles (amphitheatre-like and cone-like shapes, tectonized structures) can be identified on the main axis of PS, possibly reflecting changes of the environments of formation in terms of water column depth. These effects are typical of shoaling volcanoes, but may be also due to variations in the mechanical properties of the substratum, recorded in the passing from the deeper Marsili plain to the shallower escarpment.
- Lateral collapses may have been active both on the northern and on the southern flanks of the PS. Some of the CZ valleys could have been produced by lateral spreading phenomena.
- The adoption of major and minor Piotr's cones as names to identify the top features of PS is proposed. Flat-topped surfaces of these two features may be related to the presence of marine terraces over the top of Piotr's cones due to erosional processes related to the last eustatic sea-level lowering.
- The main fault affecting the top of PS strikes N65°E, but evidence of E–W and N–S faults is also found. The main N65°E fault may have controlled the arrangement of the younger SE sector of the seamount. With regard to this structure, a right-lateral component of movement may be inferred.
- Considering that PS is aligned along a N100°E and assuming that the E–W deep-seated structure which has controlled its emplacement moved as a sinistral strike-slip system, structure evolution of the PS could be interpreted as a conjugate fracture system with different generations of fractures, based on a sequential opening-mode. The E–W deep-seated structure could be interpreted as the main fracture (the oldest) of the network, the N65°E fault can be interpreted as a second generation of faults, characterized by a right-lateral component of movement. The N–S fault system (e.g., EZ) as left-lateral faults related to right-lateral movement of the N65°E second generation, thus represents a third generation of fractures.
- The new DTM of PS shows a very complex morphology. Although some of the proposed hypothesis must be corroborated by further geophysical investigation, data presented here may offer new constraints towards a better understanding of regional volcanism and geodynamical processes of the southeastern Tyrrhenian Sea.

Acknowledgments

We sincerely thank Guido Ventura and an anonymous reviewer for their helpful comments and suggestions and Andrew Plater, Editor, for the precious editorial handling.

Please cite this article as: Passaro, S., et al., DTM-based morphometry of the Palinuro seamount (Eastern Tyrrhenian Sea): Geomorphological and volcanological implications, Geomorphology (2009), doi:10.1016/j.geomorph.2009.09.041

References

Amante, C., Eakins, B. W., 2008. ETOPO1 1 Arc-Minute Global Relief Model: procedures, data sources and analysis. National Geophysical Data Center, NESDIS, NOAA, U.S. Department of Commerce, Boulder, CO.

Argnani, A., Savelli, C., 2001. Magmatic signature of episodic back-arc rifting in the southern Tyrrhenian Sea, in Peri-Tethyan Rift/Wrench basins and passive margins. Peri-Tethys Mem. 6: In: Ziegler, P.A., et al. (Ed.), Mem. Mus. Natl. Hist. Nat., 186, pp. 735–754.

Beccaluva, L., Gabbianelli, G., Lucchini, F., Rossi, P.L., Savelli, C., 1985. Petrology and K/Ar ages of volcanic dredged from the Eolian seamounts: implications for geodynamic evolution of the Southern Tyhrrenian basin. Earth Planet. Sci. Lett. 74, 187–208.

Beccaluva, L., Rossi, P.L., Serri, G., 1982. Neogene to Recent volcanism of the Southern Tyrrhenian–Sicilian area: implications for the geodynamic evolution of the Calabrian Arc. Earth Evol. Sci. 3, 222–238.

Bonatti, E., Bortoluzzi, G., Carrara, G., Faretti, P., Gasperini, L., Ligi, M., Marani, M., Penitenti, D., Trincardi, F., Zitellini, N., 1997. Il Tirreno, l'Oceano Periartico, l'Atlantico equatoriale: primi risultati di tre spedizioni. Annual Meeting of Gruppo Nazionale per la Vulcanologia (GNV) of Italy, Rome. March 3–5, 1997.

Bourillet, J.F., Edy, C., Rambert, F., Satra, C., Loubrieu, B., 1996. Swath mapping system processing: bathymetry and cartography. Mar. Geophys. Res. 18, 487–506.

Carminati, E., Wortel, M.J.R., Spakman, W., Saladini, R., 1998. The role of slab detachment processes in the opening of the western-central Mediterranean basins: some geological and geophysical evidence. Earth Planet. Sci. Lett. 160, 651–665.

Carracedo, J.C., 1996. A simple model for the genesis of large gravitational landslide hazards in the Canary Islands. In: McGuire, W.J., Jones, A.P., Neuberg, J. (Eds.), Volcano Instability on the Earth and Other Planets: Geol. Soc. London, Spec. Pub., vol. 110, pp. 125–135.

Cecchi, E, van Wyk de Vries, B., Lavest, J.-M., 2005. Flank spreading and collapse of weak-cored volcanoes. Bull Volc 67, 72–91.

Charlou, J.L., Donval, J.P., Zitter, T., Roy, N., Jean-Baptiste, P., Foucher, J.P., Woodside, J., MEDINAUT Scientific Party, 2003. Evidence of methane venting and geochemistry of brines on mud volcanoes of the eastern Mediterranean Sea. Deep-Sea Res. 50, 941–958.

Chiarabba, C., De Gori, P., Speranza, F., 2008. The southern Tyrrhenian subduction zone: deep geometry, magmatism and Plio-Pleistocene evolution. Earth Planet. Sci. Lett. 268, 408–423.

Ciabatti, M., 1970. Sedimenti dei monti sottomarini. Ricerche geologiche preliminari nel Mar Tirreno: In: Selli (Ed.), G. Geol., vol. 37, pp. 73–88.

Colantoni, P., Lucchini, F., Rossi, P.L., Sartori, R., Savelli, C., 1981. The Palinuro volcano and magmatism of the southeastern Tyrrhenian Sea (Mediterranean). Mar. Geol. 39, M1–M12.

de Alteriis, G., Passaro, S., Tonielli, R., 2003. New, high resolution swath bathymetry of Gettysburg and Ormonde Seamounts (Gorringe Bank, eastern Atlantic) and first geological results. Mar. Geophys. Res. 24, 223–244.

De Astis, G., Ventura, G., Vilardo, G., 2003. Geodynamic significance of the Aeolian volcanism (Southern Tyrrhenian Sea, Italy) in light of structural, seismological, and geochemical data. Tectonics 22 (4), 1040–1057.

Dekov, V.M., Savelli, C., 2004. Hydrothermal activity in the SE Tyrrhenian Sea: an overview of 30 years of research. Mar. Geol. 204, 161–185.

Del Monte, M., 1972. Il vulcanesimo del Mar Tirreno- nota preliminare sui vulcani Marsili e Palinuro. G. Geol. 38, 231–252.

Della Vedova, B., Pellis, G., Foucher, J.P., Rhéault, J.-P., 1984. Geothermal structure of the Tyrrhenian Sea. Mar. Geol. 55, 271–289.

Di Girolamo, P., 1978. Geotectonic settings of Miocene-Quaternary volcanism and around the Eastern Tyrrhenian Sea border (Italy) as deduced from the Major Element. Geochemistry Bull. Volcanol. 41 (3), 1–22.

Fabbri, A., Marabini, F., Rossi, S., 1973. Lineamenti geomorfologici del Monte Palinuro e del Monte delle Baronie (Mar Tirreno). G. Geol. 39, 133–156.

Faccenna, C., Becker, T.W., Lucente, F.P., Jolivet, L., Rossetti, F., 2001. History of subduction and back-arc extension in the Central Mediterranean. Geophys. J. Int. 145, 809–820.

Finetti, I., 2005. Deep seismic exploration of the Central Mediterranean and Italy. Elsevier, Amsterdam. 794 pp.

Flodin, E.A., Aydin, A., 2004. Evolution of a strike-slip fault network, Valley of Fire, southern Nevada. Geol. Soc. Am. Bull. 116, 42–59.

Gamberi, F., Marani, M., Landuzzi, V., Magagnali, A., Penitenti, D., Rosi, M., Bertagnini, A., Di Roberto, A., 2006. Sedimentologic and volcanologic investigation of the deep Tyrrhenian Sea: preliminary results of cruise VST02. Ann. Geophys. 49, 767–781.

Gamberi, F., Marani, M., Savelli, C., 1997. Tectonic, volcanic and hydrothermal features of a submarine portion of the Aeolian arc (Tyrrhenian Sea). Mar. Geol. 140, 167–181.

Gardner, J.M., 2001. Mud volcanoes revealed and sampled on the Western Moroccan continental margin. Geophys. Res. Lett. 28, 339–342.

Goes, S., Giardini, D., Jenny, S., Hollenstein, C., Kahle, H.-G., Geiger, A., 2006. A recent tectonic reorganization in the South-Central Mediterranean. Earth Planet. Sci. Lett. 225, 335–345.

Guarnieri, P., 2006. Plio-Quaternary segmentation of the south Tyrrhenian forearc basin. Int. J. Earth Sci. (Geol. Rundsch.) 95, 107–118.

Guth, P.L., 2003. Terrain organization calculated from digital elevation models. In: Evans, I.S., Dikau, R., Tokunaga, E., Ohmori, H., Hirano, M. (Eds.), Concepts and Modelling in Geomorphology: International Perspectives. Terrapub Publishers, Tokyo, pp. 199–220.

Gvirtzman, Z., Nur, A., 1999. The formation of Mount Etna as the consequence of slab rollback. Nature 401, 782–785.

Gvirtzman, Z., Nur, A., 2001. Residual topography, lithospheric structure and sunken slabs in the Central Mediterranean. Earth Planet. Sci. Lett. 187, 117–130.

Head III, J.W., Wilson, L., 2003. Deep submarine pyroclastic eruptions: theory and predicted landforms and deposits. J. Volcanol. Geoth. Res. 121, 155–193.

Hodgson, M.E., 1998. Comparison of angles from surface slope/aspect algorithms. Cartogr. Geogr. Inf. Syst. 25, 173–185.

Huguen, C., Mascle, J., Woodside, J., Zitter, T., Foucher, J.P., 2005. Mud volcanoes and mud domes of the Central Mediterranean Ridge: near-bottom and in situ observations. Deep-Sea Res. 52, 1911–1931.

IHO Special Publ. N° 44, 1998. Standards for Hydrographic Surveys, International Hydrographic Bureau, Monaco4th Edition.

Johnson, K.T.M., Graham, D.W., Rubin, K.H., Nicolaysen, K., Scheirer, D.S., Forsyth, D.W., Baker, E.T., Douglas-Priebe, L.M., 2008. Boomerang Seamount: the active expression of the Amsterdam-St. Paul hotspot, Southeast Indian Ridge. Earth Planet. Sci. Lett. 183, 245–259.

Kastens, K., Mascle, J., Auroux, C., Coll. ODP Leg 107 Scientific Party, 1988. ODP Leg 107 in the Tyrrhenian sea: insights into passive margin and back-arc basin evolution. Geol. Soc. Amer. Bull. 100, 1140–1156.

Kastens, K.A., Mascle, J., et al., 1990. Proc. ODP, Sci. Results. Ocean Drilling Program, College Station, TX, vol. 107.

Kidd, R.B., Armansson, H., 1979. Manganese and iron micronodules from a volcanic seamount in the Tyrrhenian Sea. J. Geol. Soc. London 136, 71–76.

Lambeck, K., Antonioli, F., Purcell, A., Silenzi, S., 2004. Sea-level change along the Italian coast for the past 10.000 yr. Quat. Sci. Rev. 23, 1567–1598.

Malinverno, A., Ryan, W.B.F., 1986. Extension in the Tyrrhenian Sea and shortening in the Apennines as a result of arc migration driven by sinking of the lithosphere. Tectonics 5, 227–245.

Mantovani, E., Babbucci, D., Tamburelli, C., Viti, M., 2008. A review on the driving mechanism of the Tyrrhenian–Apennines system: Implications for the present seismotectonic setting in the Central-Northern Apennines. Tectonophysics. doi:10.1016/j.tecto.2008.10.032.

Marani, M.P., Gamberi, F., Bonatti, E., 2004. From seafloor to deep mantle: architecture of the Tyrrhenian backarc basin. Mem.Descr.Carta geol.d'Italia LXIV.

Marani, M.P., Trua, T., 2002. Thermal constriction and slab tearing at the origin of a super-inflated spreading ridge, Marsili Volcano (Tyrrhenian Sea). J. Geophys. Res. 107, 2188.

Marinelli, G., 1975. Magma evolution in Italy. In: Squires (Ed.), Geology of Italy, Earth Sci. Soc. of Lybian Arab Republic, Tripoli, pp. 165–219.

Mark, R., Pike, R.J., Bortoluzzi, G., Ligi, M., 1991. Mediterranean seabed in digital shaded relief. Eos Trans. AGU 72 (26), 273-273.

McPhie, J., 1995. A Pliocene shoaling basaltic seamount: Ba volcanic group at Rakiraki, Fiji. J. Volcanol. Geotherm. Res. 64, 193–210.

Mitasova, H., Hofierka, J., 1993. Interpolation by regularized spline with tension: II. Application to terrain modeling and surface geometry analysis. Math. Geol. 25, 657–669.

Montuori, C., Cimini, G.B., Favali, P., 2007. Teleseismic tomography of the southern Tyrrhenian subduction zone: new results from seafloor and land recordings. J. Geophys. Res. 112, B03311.

Moore, J.G., Mark, R.K., 1992. Morphology of the island of Hawaii. GSA Today 2, 257–262.

Moore, I.D., Lewis, A., Gallant, J.C., 1993. Terrain properties: estimation methods and scale effects. In: Jakeman, A.J., et al. (Ed.), Modeling Change in Environmental Systems. John Wiley and Sons, New York. pp.

Morelli, C., 1970. Physiography, gravity and magnetism of the Tyrrhenian Sea. Boll. Geofis. Teor. Appl. 12, 275–309.

Mukhopadhyay, R., Rajesh, M., De, S., Chakraborty, B., Jauhari, P., 2008. Structural highs on the western continental slope of India: Implications for regional tectonics. Geomorphology 96, 48–61.

Rosenbaum, G., Lister, G.S., 2004. Neogene and Quaternary rollback evolution of the Tyrrhenian Sea, the Apennines and the Sicilian Maghrebides. Tectonics 23, TC1013.

Rowland, S.K., Garbeil, H., 2000. Slopes of oceanic basalt volcanoes. In: Mouginis-Mark, P.J., Crisp, J.A., Fink, J.H. (Eds.), Remote Sensing of Active Volcanism. : Geophys. Monogr. Ser., 116. AGU, Washington, pp. 223–247.

Savelli, C., 2001. Two-stage progression of volcanism (8–0 Ma) in the central Mediterranean (southern Italy). J. Geodyn. 31, 393–410.

Savelli, C., 2002. Time-space distribution of magmatic activity in the western Mediterranean and peripheral orogens during the past 30 Ma (a stimulus to geodynamic considerations). J. Geodyn. 34, 99–126.

Scarascia, S., Lozej, A., Cassinis, R., 1994. Crustal structures of the Ligurian, Tyrrhenian and Ionian Seas and adjacent onshore areas interpreted from wide-angle seismic profiles. Boll. Geofis. Teor. Appl. 36, 5–19.

Smith, D.K., Humphris, S.E., Tivey, M.A., Cann, J.R., 1997. Viewing the morphology of the Mid-Atlantic Ridge from a new perspective. EOS. Trans. Am. Geophys. Union 78, 265–269.

Smoot, N.C., 1995. Mass wasting and subaerial weathering in guyot formation: the Hawaiian and Canary Ridges as examples. Geomorphology 14, 29–41.

Soloviev, S.L., Kuzin, I.P., Kovachev, S.A., Ferri, M., Guerra, I., Luongo, G., 1990. Microearthquakes in the Tyrrhenian Sea as revealed by joint land and sea-bottom seismographs. Mar. Geol. 94, 131–146.

Suhadolc, P., Panza, G.F., 1989. Physical properties of the lithosphere–asthenosphere system in Europe from geophysical data. Proceedings of 'The lithosphere in Italy'. Accad. Naz. Lincei 80, 15–40.

Thouret, J.-C., 1999. Volcanic geomorphology—an overview. Earth-Sci. Rev. 47, 95–131.

Turco, E., Zuppetta, A., 1998. A kinematic model for the Plio-Quaternary evolution of the Tyrrhenian–Apenninic system: implications for rifting processes and volcanism. J. Volcanol. Geoth. Res. 82, 1–18.

Yokoyama, R., Sirasawa, M., Pike, R.J., 2002. Visualizing topography by openness: a new application of image processing to digital elevation models. Photogramm. Eng. Remote Sensing 68, 257–265.

Zitter, T.A.C., Huguen, C., Woodside, J.M., 2005. Geology of mud volcanoes in the eastern Mediterranean from combined sidescan sonar and submersible surveys. Deep-Sea Res. 52, 457–475.

Please cite this article as: Passaro, S., et al., DTM-based morphometry of the Palinuro seamount (Eastern Tyrrhenian Sea): Geomorphological and volcanological implications, Geomorphology (2009), doi:10.1016/j.geomorph.2009.09.041